AIIM

Association for Information and Image Management

1100 Wayne Avenue, Suite 1100
Silver Spring, Maryland 20910

301/587-8202

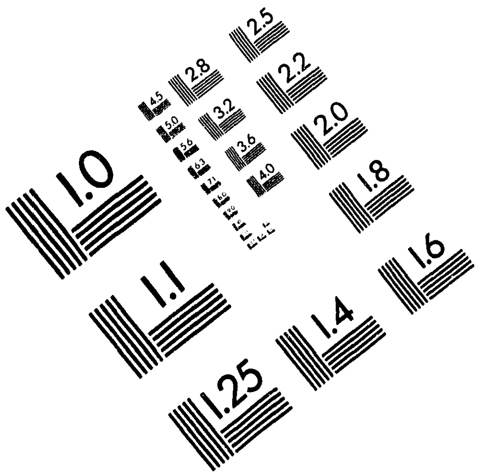

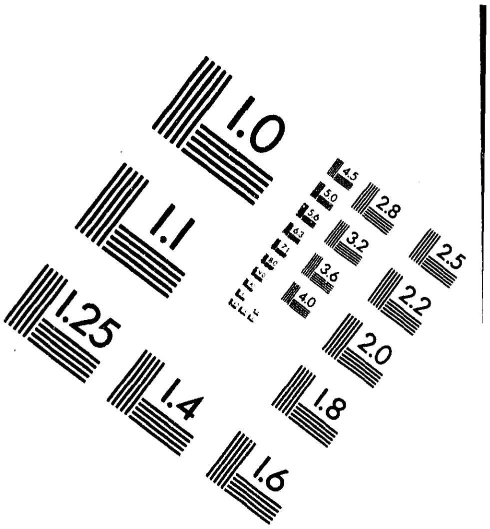

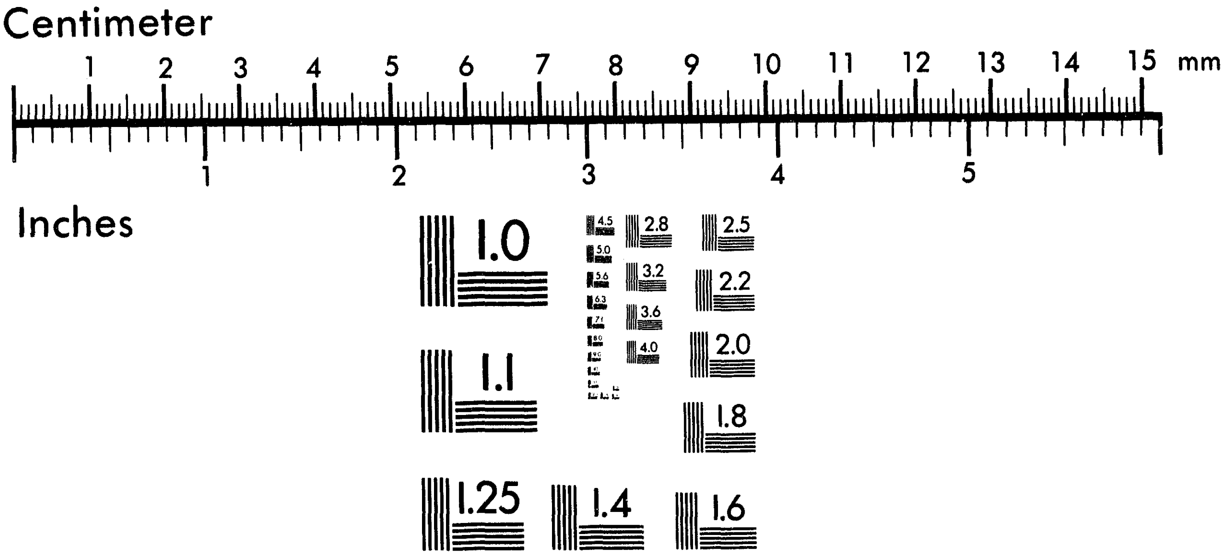

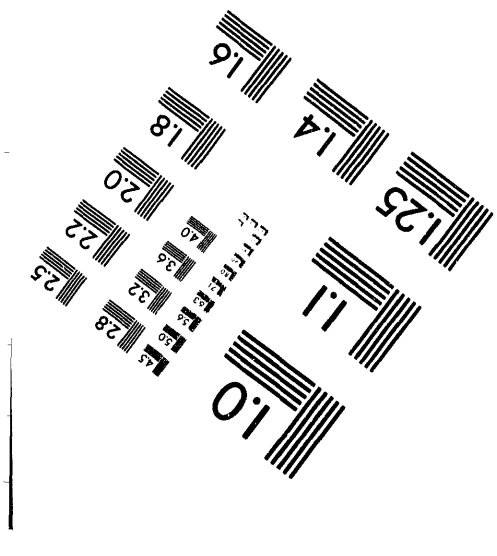

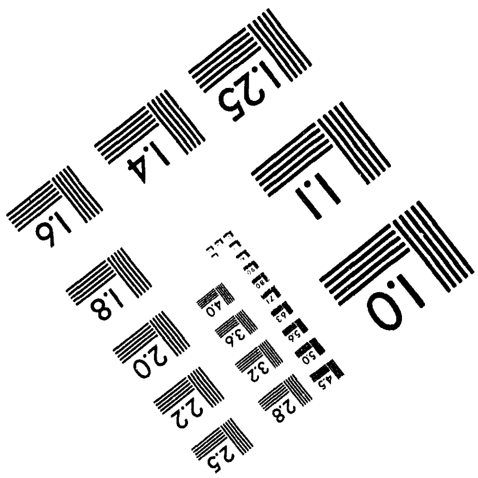

MANUFACTURED TO AIIM STANDARDS

BY APPLIED IMAGE, INC.

1 of 1

THE APPLICATION OF COMPUTATIONAL SIMULATION TO DESIGN OPTIMIZATION OF AN AXISYMMETRIC RAPID THERMAL PROCESSING SYSTEM

Paul A. Spence, William S. Winters, and Robert J. Kee
Sandia National Laboratories
Livermore, CA, 94551-0969

Ahmad Kermani
CVC Products, Inc.
47061 Warm Spring Blvd., Fremont, CA 94539

We are developing and applying computational models to guide the development of a rapid-thermal-processing system. This work concentrates on scale-up and commercialization of the axisymmetric, multiple-lamp-ring approach that was pioneered by Texas Instruments in the Microelectronics Manufacturing Science and Technology program. CVC Products intends to incorporate the tool into their open-architecture MESC compatible cluster environment. Integration of modeling into the product development process can reduce time-to-market and development costs, as well as improve tool performance.

INTRODUCTION

It has been demonstrated in many industrial situations that analytic and computer modeling can reduce the time and cost required for equipment design while improving product performance. Because of the difficulty in achieving and controlling process uniformity in rapid-thermal-processing (RTP) systems, modeling can play an important role in advancing the technology to meet or exceed market requirements.

The work discussed here focuses on the application of Sandia-developed models to guide the design of an RTP reactor. Sandia National Laboratories and CVC Products, Incorporated are working together to implement computational simulation as an integral part of their development process. We have used numerical models in the design analysis of the CVC Universal Thermal Module, which is a scaled up and enhanced version of the RTP system developed for the Microelectronics Manufacturing Science and Technology (MMST) program at Texas Instruments [1]. Our approach considers both conduction-radiation heat transfer simulations and fluid flow simulations. The axisymmetric geometry allows simulations to be done in two-dimensions, which greatly reduces model simulation times when compared to the CPU time requirements for three-dimensional simulations.

Specifically, this paper addresses the use of models to optimize the design of two critical reactor features: (1) the reactor lamp housing and (2) the reaction chamber (including the showerhead gas injector). The lamp housing must supply radiant heat to the wafer such that temperature uniformity can be maintained during both steady and transient conditions. Due to the highly nonlinear thermal characteristics of the RTP system, the radiant flux distribution required for temperature uniformity varies with operating temperature, making controllability an important design consideration. We have applied finite-element thermal models to guide the design of the lamp housing in terms of power requirements, lamp-zone positions, and system controllability.

The reaction chamber must be designed to insure uniform wafer deposition. Gas delivery systems that produce ideal stagnation-type flows will achieve uniform reactant fluxes at the wafer surface [2]. The ability to achieve an ideal stagnation flow depends on

inlet-flow uniformity and characteristic reaction-chamber dimensions such as inlet diameter and inlet-to-wafer distance as well as the process operating conditions. The showerhead injector is a critical part of the gas-delivery system and must be designed to deliver a uniform flow rate across the inlet diameter. The chamber geometry must also provide for a sufficient gas mixing length so that the showerhead hole pattern is not imaged on the wafer. With these concerns in mind, we have applied both dimensional analysis techniques and Navier-Stokes simulations to the design of the reaction chamber and showerhead.

REACTOR DESCRIPTION

The RTP reactor currently in development at CVC is an axisymmetric design with five independently controlled lamp zones that heat the back side of a 200 mm wafer. Figure 1 shows a schematic representation of the reactor geometry. Each lamp zone contains an array of tungsten-halogen bulbs arranged in a circular pattern. Between each lamp zone is a radiation partition which limits "cross-talk" between the zones for improved control characteristics. The wafer rests face-up on a support that is attached to a rotation mechanism. Reactant gases are delivered through a multi-zone showerhead manifold from the top of the reactor. The face of the showerhead is polished for high reflectivity, creating a condition that approaches the behavior of a black-body cavity, and thereby reducing the sensitivity of the system to wafer front-side emissivity variations. A quartz window separates the lamp housing from the reaction chamber and the wafer. The chamber walls are water cooled. Deposition of reactants on the wafer back side and the window during processing is prevented by the wafer support ring. The reaction chamber is designed with a Modular Equipment Standards Committee (MESC) compatible interface.

A typical process run begins with a controlled ramp (10-100 °C/s) to the process set-point temperature. Temperature is measured continually during the process with a multi-point fiber-optic IR pyrometry system. Once the wafer temperature is stabilized, the process gas enters the reactor through the showerhead injector. During this phase of the process, it is critical that the temperature control system maintain wafer temperature uniformity. Because of long thermal time constants in the system (i.e. slow heat up of the window and walls), the power applied to the lamps must be continually adjusted. When the wafer processing is finished, temperature is ramped down and the wafer is removed from the reactor.

MODELING APPROACH AND BOUNDARY CONDITIONS

The heat-transfer analysis uses the Sandia-developed TACO software [3], which is a two- or three-dimensional finite-element code. Radiant heat exchange between enclosure surfaces is based on the net radiation method [4]. View factors for the enclosure radiation exchange are computed using the VIEWC software [5]. Typical thermal simulations for the RTP system have approximately 1000 elements and 400 radiation surfaces.

The quartz window dividing the lamps from the wafer has a significant thermal effect on the system. Including the window in the model is complicated by the need for a non-gray (wavelength dependent) radiation model to account for the semi-transparent behavior of quartz (Fig. 2). Because our finite-element model treats all surfaces as gray-diffuse, we implemented a technique to capture the thermal effect of the window. This is done by an alternate treatment of the view factors. First, three radiation enclosures are defined as shown in Fig. 3. Enclosure 1 includes the surfaces above the window (wafer, support, wall) and the top surface of the window. Enclosure 2 includes the surfaces below the window (lamps, radiation partitions, wall) and the bottom surface of the window.

Enclosure 3 includes all surfaces in enclosures 1 and 2 except the window. Gray-diffuse view factors are computed independently for each of these three enclosures. Next, the three sets of view factors are combined into one global set, insuring that the summation of view factors for each surface equals unity. To account for the semi-transparent window, all view factors across the window (i.e. lamps to wafer) are multiplied by the quartz transmissivity, τ, and all view factors to the window are multiplied by $1-\tau$. By using two quartz transmissivities, one value for energy leaving the wafer and a second value for energy leaving the lamps, we effectively create a two-band radiation model that accounts for the wavelength dependency of quartz. "Lumped" transmissivity values are chosen that account for the combined wavelength spectrum of both emitted and reflected radiation. Figure 2 shows the wavelength spectrum of energy emitted from the lamps (2700 °C) and wafer (600 °C) along with a plot of the quartz transmissivity variation with wavelength.

Heat is removed from the model through convective boundary conditions that account for air cooling inside the lamp housing and for water cooling on the outer chamber walls. Heat input to the model is through volumetric heat generation (W/m^3) in the lamp zones. An annular ring approximation is used to represent the discrete lamps of each zone. The heat generation is controlled independently for each lamp zone.

The fluid-flow and convective-heat-transfer analysis is based on Sandia's CURRENT software, which is a two-dimensional code for the solution of the Navier-Stokes, energy, and species conservation equations. The conservation equations are integrated over control volumes and the remaining derivatives are discretized using finite differences. Solution of the equations is obtained using the SIMPLER method [6] and the tridiagonal matrix algorithm. The use of multiple regions and non-orthogonal grids permits economical simulation of complex geometries. The ideal-gas equation of state relates the gas density and temperature, assuming a nominal thermodynamic pressure. Temperatures obtained from finite-element thermal simulations are applied to the wafer, chamber walls, and showerhead as boundary conditions for the gas flow simulations.

In addition to the Navier-Stokes simulations, a dimensional analysis was used to help identify stable flow regimes in the large parameter space considered. Figure 4 shows the characteristic parameters that describe reaction chamber flow conditions. Using these parameters we define the Reynolds number as

$$\mathrm{Re} = \frac{D_i V_i \rho}{\mu} \qquad (1)$$

and the Grashof number as

$$\mathrm{Gr} = \frac{g\beta L^3 (T_{\mathrm{wafer}} - T_{\mathrm{i}})\rho^2}{\mu^2}. \qquad (2)$$

where D_i is the gas inlet diameter, V_i is the average gas inlet velocity, L is the inlet-to-wafer distance, and T_{wafer} and T_{i} are the wafer and inlet temperatures. Gas properties are represented by density (ρ), viscosity (μ), and the thermal expansion coefficient (β), all

evaluated at the inlet temperature. A third dimensionless parameter is the mixed-convection parameter [7]

$$\frac{\mathrm{Gr}}{\mathrm{Re}^2} = \frac{gL^3(T_{\mathrm{wafer}} - T_{\mathrm{i}})}{T_{\mathrm{i}}(D_{\mathrm{i}}V_{\mathrm{i}})^2}. \qquad (3)$$

where $\beta = 1/T_{\mathrm{i}}$ for an ideal gas. The mixed-convection parameter represents the ratio of the square of free convection velocity to forced convection velocity in a system. It has been shown, for this class of reactor, that operation with mixed-convection parameter values less than unity will lead to forced stagnation-like flows with no destabilizing buoyant recirculations [7].

RESULTS

Thermal Modeling

Design analysis of the reactor lamp housing was done using both steady-state and transient simulations along with techniques to determine system controllability and temperature-uniformity limits. The starting point for the lamp-housing design was the 4-zone, 65 kilowatt lamp configuration developed for the MMST program. The MMST reactor was designed to process 150 mm wafers; however, we used the MMST lamp configuration with 200 mm wafers in our simulation as a basis for comparison with other 4 and 5-zone lamp configurations. One of the first things considered was the power requirements for the 200 mm system. Since the highest power demand is during thermal ramps, we simulated wafer-temperature ramps from 500 °C to 1100 °C at approximately 70 °C/second. Figure 5 shows a series of wafer-temperature profiles at discrete times during the ramp for both the MMST 65 kW lamp design and a five zone 109 kW lamp design. Figure 6 compares the lamp-power trajectories of the outer lamp zone for the two transient simulations. Figures 5 and 6 show that the MMST lamp design is unable to provide sufficient power to the wafer edge to maintain temperature uniformity during high ramp rates.

Computation of the steady-state (or DC) gain matrix of the system is a useful method for evaluating the controllability of a given lamp design. The gain is represented by

$$k_{i,j} = \frac{\Delta T_i}{\Delta P_j} \qquad (4)$$

where ΔT_i denotes the change in temperature at point i on the wafer and ΔP_j denotes the change in power of lamp zone j [8]. The gain matrix is calculated at several operating temperatures between 500 and 1100 °C. For this system, gain (i.e. change in wafer temperature for a 1% change in power) decreases with temperature. Figure 7 shows "gain profiles" associated with the center lamp zone for wafer temperatures of 500, 700, 900, and 1100 °C. The gain profile is the plot of a column from the gain matrix that shows the radial variation in wafer temperature response for a 1% power change from a given lamp zone $\left(k_i(r) = \Delta T(r)/\Delta P_i\right)$. The gain matrix provides important information concerning

controllability of the system. The use of gain matrices to evaluate controllability is discussed by Cho and Kailath [9], where investigation of a gain matrix from their experimental system led to the idea of installing radiation partitions between lamp zones. We use comparison of gain profiles as a method to visually understand the effect specific design modifications have on system controllability. Figures 8a and 8b show gain profiles for a 5-zone lamp design, where the design parameter is the length of the radiation partitions that separate each lamp zone. The gain profiles show how each lamp zone will effect the wafer temperature. The reason for the increase in the magnitude of the gain from the center zone (zone 1) outward to the third zone is that the maximum power of the zones increase with zone diameter. This trend of gain increasing with zone power does not hold for the outer two zones. These zones have diameters greater than that of the wafer, resulting in a much lower heating efficiency than the inner zones.

For good controllability, each lamp zone should strongly influence one area of the wafer and diminish radially from that region. In Fig. 8a, we see that an increase in the partition length helped to better differentiate the region of influence of the lamp zones on the wafer. One problem that still remains is that both zone 4 and zone 5 (the two outer lamp zones) have their greatest influence at the wafer edge. This essentially removes one degree of freedom from the system, which may cause difficulties in developing a stable controller.

Steady-state optimization of wafer temperature proved to be an essential tool for evaluating uniformity limits of a specific design. Optimized wafer-temperature profiles are also used as a metric for comparing alternative lamp designs. The optimization method used for this study is based on one described by Norman [8]. Briefly, lamp powers are determined that minimized the mean-square difference between wafer temperature, T_{wafer}, and the desired temperature T_{set},

$$\min_{P} \int_{0}^{R} \left(T_{wafer}(r;P) - T_{set}\right)^2 dr \qquad (5)$$

where $T_{wafer}(r;P)$ is the steady-state wafer temperature at radius r when the lamp powers are held at the values indicated by the vector P. The optimal powers are determined iteratively utilizing the gain matrix discussed earlier. For given powers and their associated temperature profile, corrections to the powers are predicted by solving the linear least squares problem

$$\min_{\Delta P} \left\| K\Delta P - (T_{wafer} - T_{set}) \right\|_2 \qquad (6)$$

where K is the $m \times n$ gain matrix ($K=[k_{i,j}]$), ΔP is a vector of corrections to the n powers, and $T_{wafer} - T_{set}$ is a vector of temperature deviations sampled at m radial locations. The powers are then corrected to $P + \Delta P$, and the process is repeated for a few iterations until the powers and temperatures cease changing.

Figure 9 shows a comparison of optimized wafer temperature profiles for three different lamp configurations. This result shows that the MMST lamp configuration (designed for 150 mm wafers) does not provide as good temperature uniformity as the 5-zone and

modified 4-zone lamp configurations. The modified 4-zone configuration is identical to the MMST design except the diameter of the outer two lamp zones are increased (with the maximum zone powers being increased accordingly) to account for the larger wafer size. Figure 10 shows that the optimized temperature uniformity degrades with temperature. The worst temperature uniformity occurs at the highest operating temperature. Figure 11 shows the power levels associated with the steady-state wafer temperatures shown in Fig. 10. Note that the relative importance of the outer lamp increases significantly with temperature.

Fluid Flow Modeling

Fluid flow analysis was used to guide the design of a reaction chamber and showerhead gas injector. Since process conditions have a strong effect on fluid flow in the chamber, design analysis must consider all intended process conditions. The process conditions considered for this system ranged from 1-760 torr for pressure, 0.5-10 slpm for flow rate, and 500-1000 °C for temperature. Simulations were done assuming gas properties of N_2, Ar, O_2, H_2, or NH_3.

This parameter space is quite large especially when combined with possible variations in the chamber geometry. To reduce the parameter space that requires detailed Navier-Stokes simulations, we applied the previously described dimensional analysis techniques. For the purpose of design analysis, we establish radial heat flux uniformity across the wafer as the figure of merit for a particular reactor design. For transport-limited deposition conditions, a strong analogy exists between heat and mass transfer provided the boundary conditions are similar. When surface chemistry is the rate-limiting step, then reactors designed by the heat-transfer analogy are more conservative than necessary.

Using the mixed convection parameter (Eq. 3), we were able to identify the conditions that resulted in both desirable and undesirable flow regimes. Conditions that yield a mixed convection parameter value less than one ($Gr/Re^2 < 1$) result in forced convection dominated flow and radially uniform fluxes at the wafer. Conditions that yield a mixed convection parameter greater than one ($Gr/Re^2 > 1$) result in buoyancy forces, flow recirculation, and nonuniform flux distributions across the wafer. The dimensional analysis was confirmed using selective Navier-Stokes simulations. Figures 12a, 12b, and 12c show steady-state streamlines and temperature isotherms for mixed convection values of 0.7, 13, and 441 respectively. The result shown in Fig. 12a is a stagnation-like flow that results in a very uniform heat flux at the wafer surface. The results shown in Figs. 12b and 12c demonstrate the effect of increasing the relative buoyancy in the system. For the conditions that produce large buoyancy forces ($Gr/Re^2 >> 1$), the heat flux is very nonuniform. This is most easily seen in Fig. 13 which shows the normalized heat flux profiles at the wafer surface for the conditions shown in Figs. 12a, 12b, and 12c.

Having utilized dimensional analysis to identify stable operating regimes within the large parameter space, the next step in the numerical design process is to address two-dimensional geometry effects using detailed Navier-Stokes calculations. First, we examine the influence of increasing the inlet flow diameter. Figure 14 illustrates the improvement in wafer heat flux uniformity which results from varying inlet flow area. For larger inlet flow areas, the "ideal" one-dimensional stagnation flow situation applies over a larger radius, thus leading to reduced two-dimensional edge effects and improved heat flux uniformity.

Similar improvements are possible by reducing the distance between the showerhead and the wafer. This trend is illustrated in Fig. 15. Actually, reducing the inlet-to-wafer distance improves heat flux uniformity for two reasons: (1) it reduces edge effects , and (2) it

reduces buoyancy effects (Eq. 3). One might conclude that the best design would be one in which the showerhead is extremely close to the wafer. This is not the case, however, since a minimum mixing distance must be maintained in order to prevent individual jets from the showerhead from influencing flux uniformity at the wafer.

A two-dimensional axisymmetric model was developed to predict the mixing length required to insure that the wafer would not be influenced by localized showerhead jetting. The model represents the flow through only one hole located along the showerhead centerline with a surrounding support flow that represents the average flow from the remaining showerhead holes. The critical parameters for this calculation are shown in Fig. 16. Assuming the hole pattern to be a close-packed-hexagonal configuration, it can be shown that the showerhead support velocity is given by

$$V_i = \frac{4\dot{m}}{\rho_i \pi D_i^2} \tag{7}$$

and the inlet-hole velocity

$$v_o = \frac{2\sqrt{3}S^2 V_i}{\pi d_o^2} \tag{8}$$

where $\dot{m}$ is the total mass flow rate, d_o is the diameter of the individual showerhead holes, S is the hole spacing, and ρ_i is the gas density at the inlet.

The two-dimensional mixing length model accounts for flow development through the showerhead plate thickness, t, by applying a uniform velocity, v_o, as a boundary condition for flow entering the centerline hole. This makes it possible to predict the resulting jet radial velocity profile as it enters the reaction chamber. The velocity, V_i, is used as a boundary condition for support flow over the remainder of the showerhead. The model includes the complete reaction chamber geometry including the wafer and walls.

Figure 17 shows the showerhead centerline velocity (i.e. hole centerline velocity) as a function of distance from the showerhead surface. Also shown in the figure is the support flow velocity which is generally independent of radius except near the outer edge of the showerhead. This result shows that for the conditions studied, approximately 1 cm is required for the jet flow to be completely merged (mixed) with the support flow. Simulations such as this are useful in estimating required mixing lengths for proposed reactor conditions and showerhead parameters (t, d_o, S).

CONCLUSIONS

We have worked closely with system designers to integrate computational simulation into CVC's design and product development process. Both thermal models and fluid-flow models were developed and used to provide design guidance. Modeling techniques were developed to simulate complex behavior within the RTP system, such as the semi-

transparent window and jetting from the showerhead holes. The use of optimization techniques, gain matrices, and dimensional analysis were essential in maximizing the value of our models.

Steady-state gain profiles were used to understand and improve system controllability. Shallow (i.e. radially independent) gain profiles and similarity between zone gain profiles can effectively reduce the degrees of freedom in the system causing control difficulties. We will continue to use models to support the development of the reactor power controller.

Steady-state optimization of wafer temperature uniformity provided a basis for comparing design alternatives. Reactor thermal characteristics were studied over the full operating range and optimal uniformity was shown to decrease as temperature increased. The radiant flux distribution required for wafer temperature uniformity was also shown to change with temperature. At high operating temperatures, wafer edge losses are significant and power from the outer lamp zone must increase to compensate for this effect.

Steady-state and transient simulations were performed; the steady-state calculations provided a basis for design comparison studies; the transient simulations provided the basis for understanding the dynamic behavior of the system. Our conclusion that the MMST lamp design was under-powered for 200 mm wafers resulted from analysis of the transient simulation.

An important aspect of the system dynamics is that wafer processing will always be done under closed-loop control. In addition to our use of gain matrices to evaluate system controllability, we have created a method of linking our finite element codes with controllers identical to those that will run the actual hardware. This allows us to perform closed-loop simulations for concurrent design of the reactor hardware and process controllers.

Fluid-flow analyses of the reaction chamber and showerhead gas injector were used to identify designs that minimized the effects of free convection and wafer edge effects and hence would result in conditions leading to uniform deposition. We used dimensional analysis to identify the processes requiring further evaluation with detailed Navier-Stokes simulations. The numerical simulations provided detailed results for gas velocity and temperature fields, distributions of wafer convective heat transfer, and verifications of the dimensional analysis results. Results from numerical parameter studies of inlet diameter, inlet-to-wafer distance, and showerhead hole jet penetration were all used by CVC to guide their design decisions.

ACKNOWLEDGMENTS

This work was sponsored by SEMATECH and the US Department of Energy.

REFERENCES

[1] M.M. Moslehi, C. Davis, and A. Bowling, *Microelectronics Manufacturing Science and Technology: Single-Wafer Thermal Processing and Wafer Cleaning*, Texas Instr. Tech. J., Vol. 9, No. 5, Sept.-Oct. 1992.

[2] E. Meeks, R.J. Kee, D.S. Dandy, and M.E. Coltrin, *Computational Simulation of Diamond Chemical Vapor Deposition in Premixed $C_2H_2/O_2/H_2$ and CH_4/O_2-Strained Flames, Combustion and Flame,* 92: 144-160, 1993.

[3] W.E. Mason, *TACO3D - A Three-Dimensional Finite Element Heat Transfer Code,* Sandia National Laboratories, 1983.

[4] R. Siegel and J.R. Howell, *Thermal Radiation Heat Transfer*, Hemisphere Publishing Corp., 1972.
[5] A.F. Emery, *View Users Manual*, Univ. of Wash., 1984.
[6] S.V. Patankar, *Numerical Heat Transfer and Fluid Flow*, McGraw-Hill, 1980.
[7] G.H. Evans and R. Greif, *A Numerical Model of the Flow and Heat Transfer in a Rotating Disk Chemical Vapor Deposition Reactor*, J. of Heat Transfer, Vol. 109, Nov. 1987.
[8] S. Norman, *Wafer Temperature Control in Rapid Thermal Processing*, Ph.D. Dissertation, Dept. of Elect. Engr., Stanford University, 1992.
[9] Y.M. Cho and T. Kailath, *Model Identification in Rapid Thermal Processing Systems*, IEEE Trans. on Semiconductor Man., Vol. 6, NO. 3, August 1993.

FIGURES

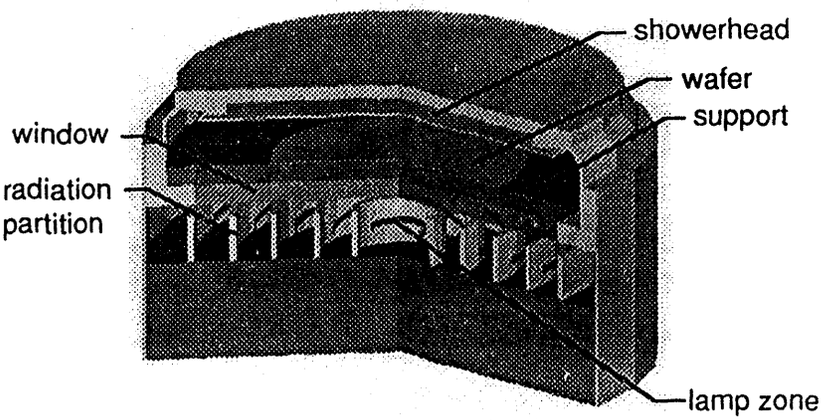

Figure 1: Model representation of the CVC RTP reactor geometry.

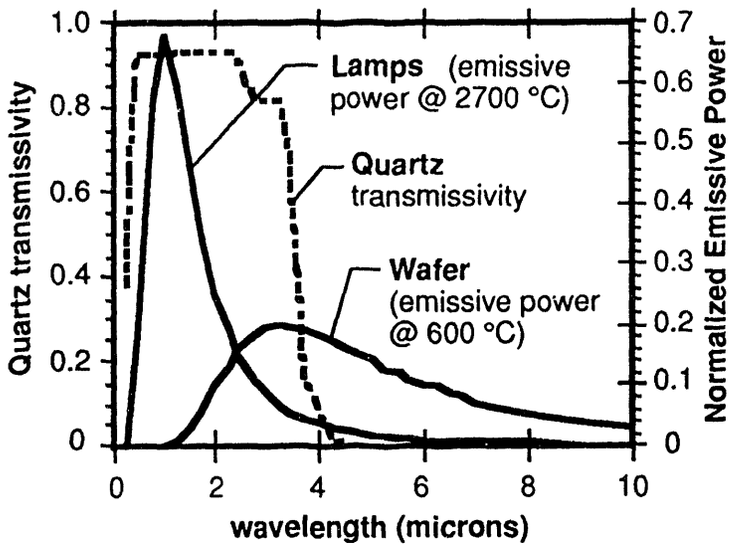

Figure 2: Wavelength dependence of quartz window transmissivity and emissive power distribution of lamps and wafer.

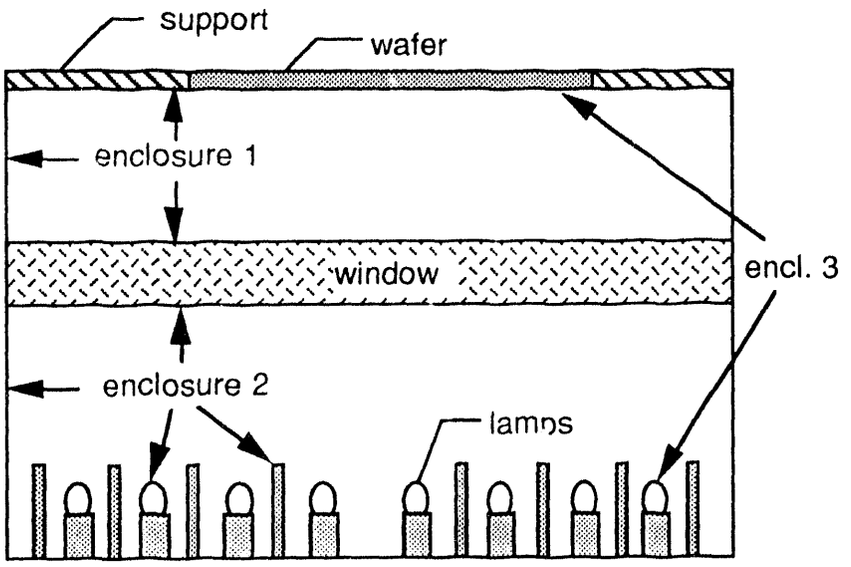

Figure 3: Radiation enclosures defined for view factor calculation. View factors from each enclosure are combined into one enclosure with a semi-transparent window.

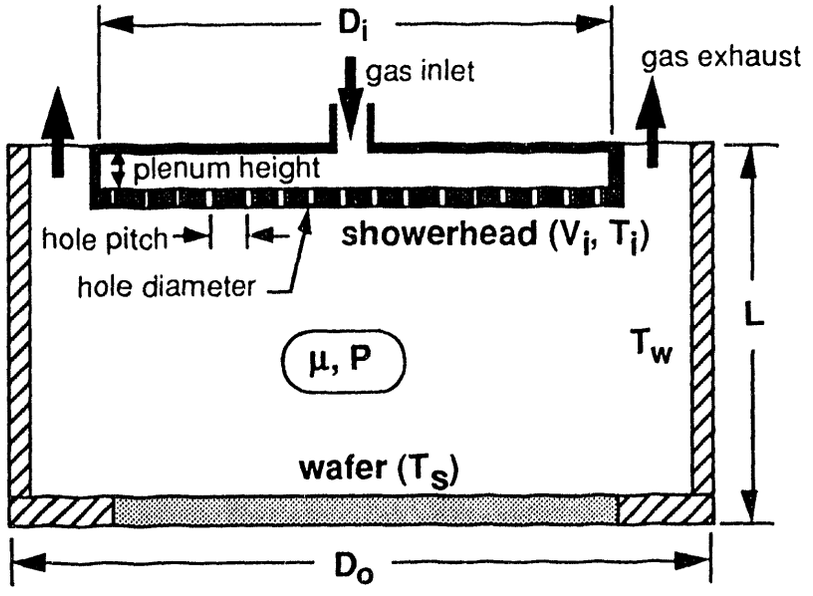

Figure 4: Characteristic parameters used in fluid flow calculations for the reaction chamber.

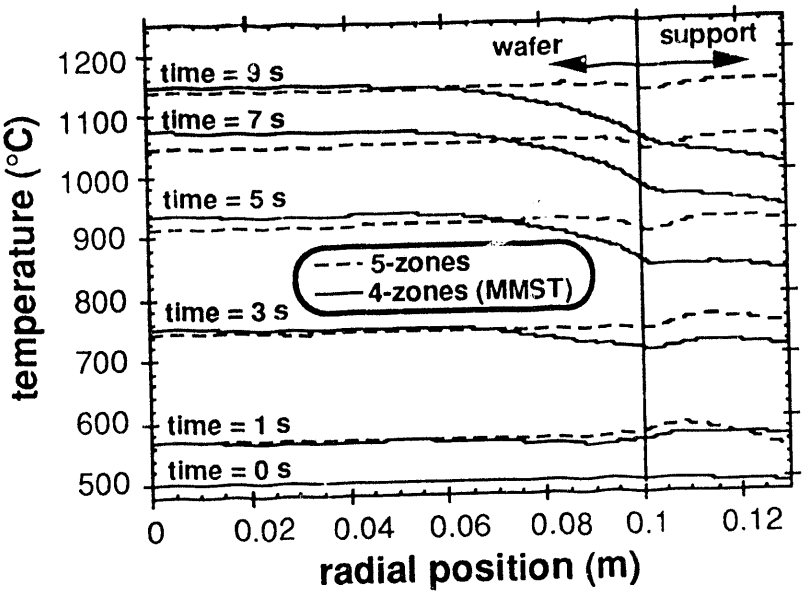

Figure 5: Wafer temperature profiles during 70 °C/s ramp for 5-zone and 4-zone (MMST) lamp configurations.

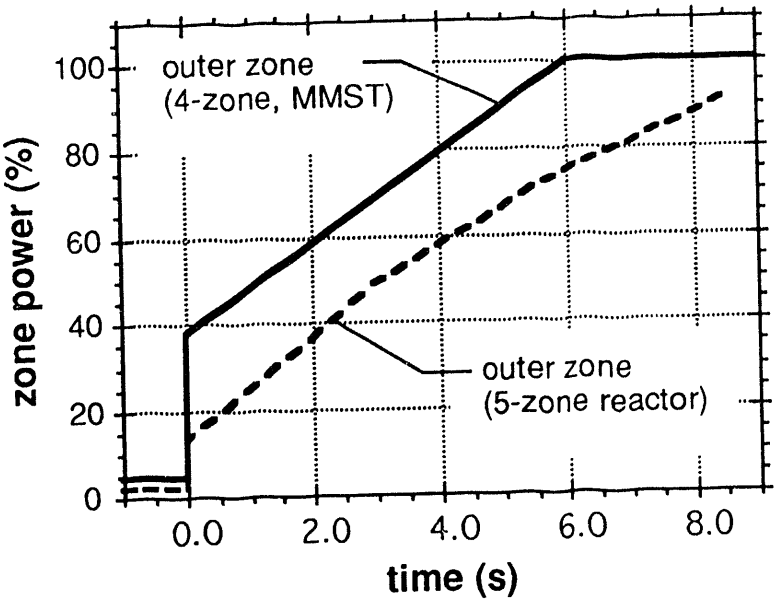

Figure 6: Power history of the outer lamp zone during 70 °C/s ramp for 5-zone and 4-zone (MMST) lamp configurations.

DISCLAIMER

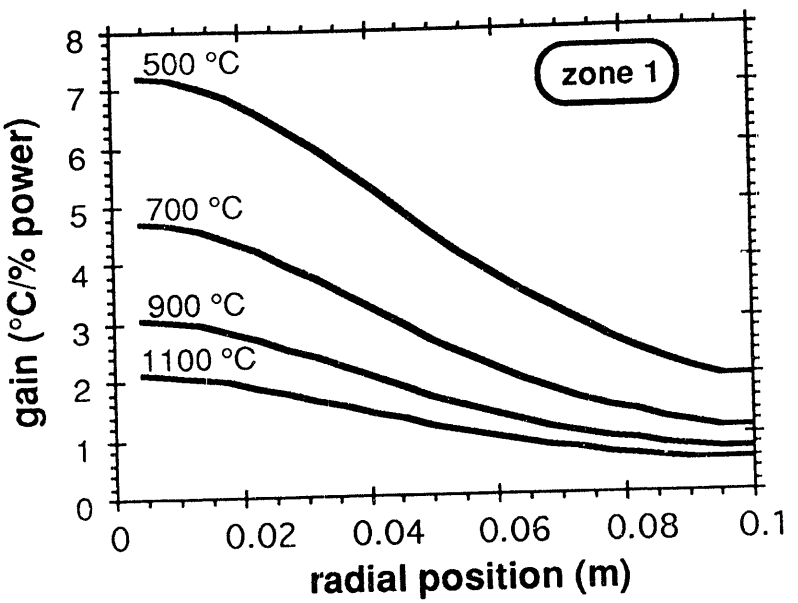

Figure 7: Change in gain associated with lamp zone 1 (center zone) with respect to wafer temperature.

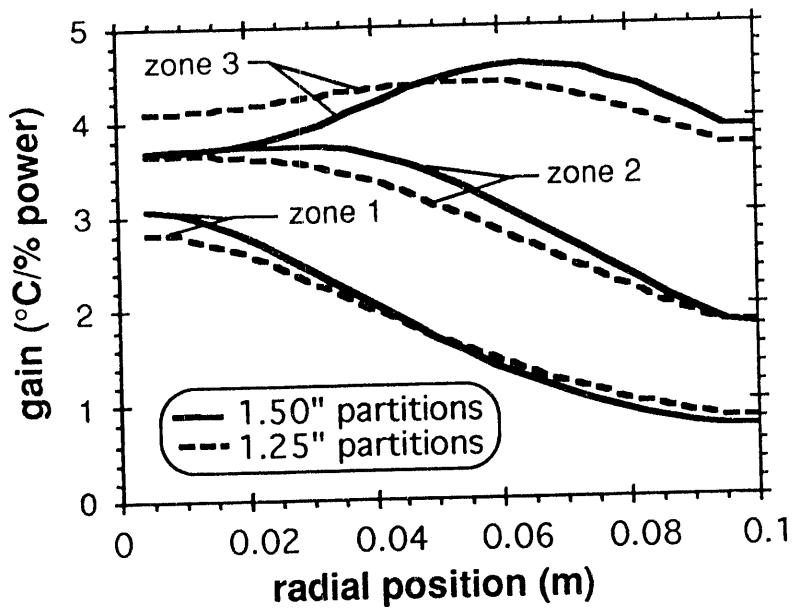

Figure 8a: Comparison of gain profiles (zones 1-3) of two 5-zone reactors with different radiation partition lengths.

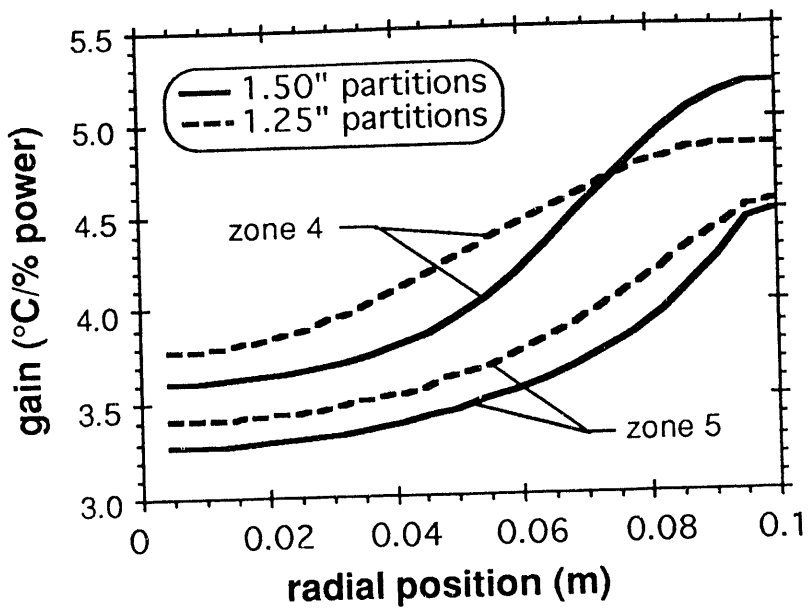

Figure 8b: Comparison of gain profiles (zones 4-5) of two 5-zone reactors with different radiation partition lengths.

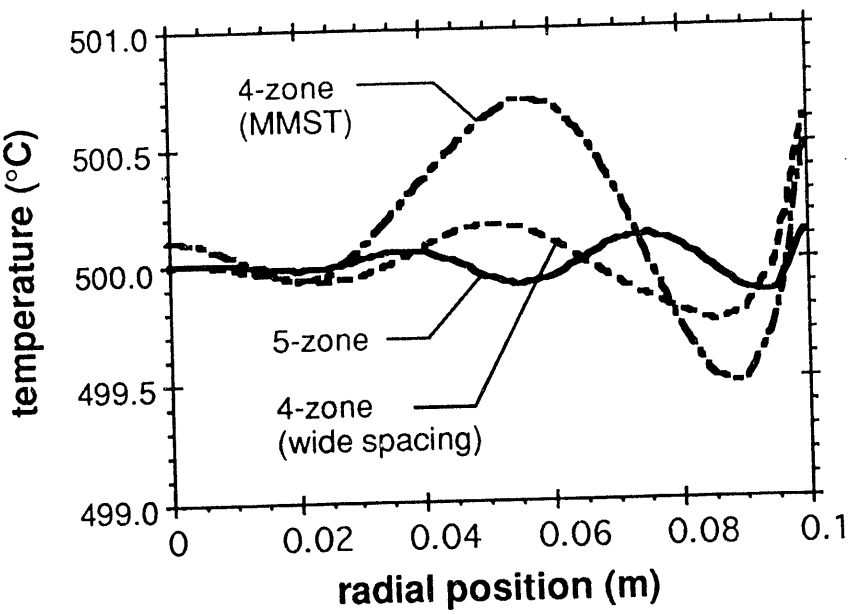

Figure 9: Optimized steady-state wafer temperature profiles (at 500 °C) for three different lamp configurations.

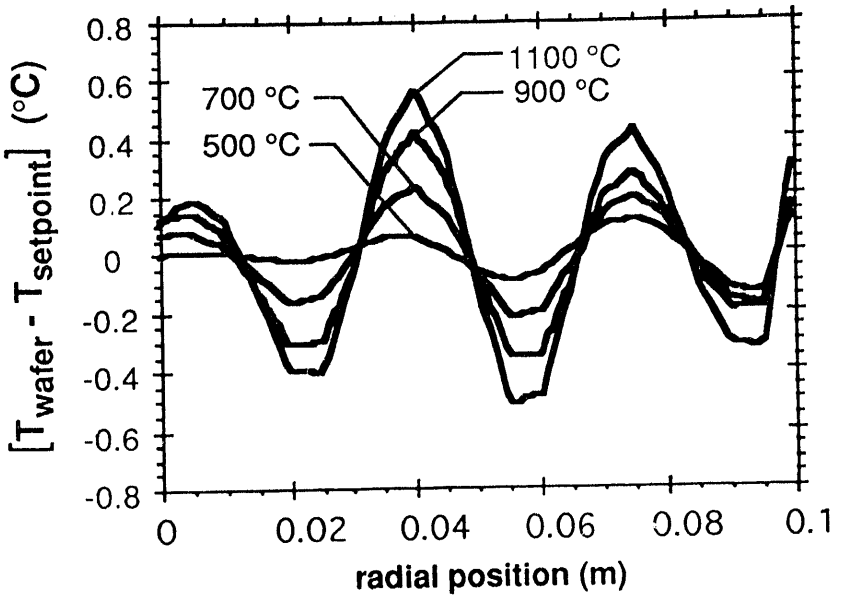

Figure 10: Wafer temperature variation from set point for a 5-zone lamp design optimized at 500, 700, 900, and 1100 °C.

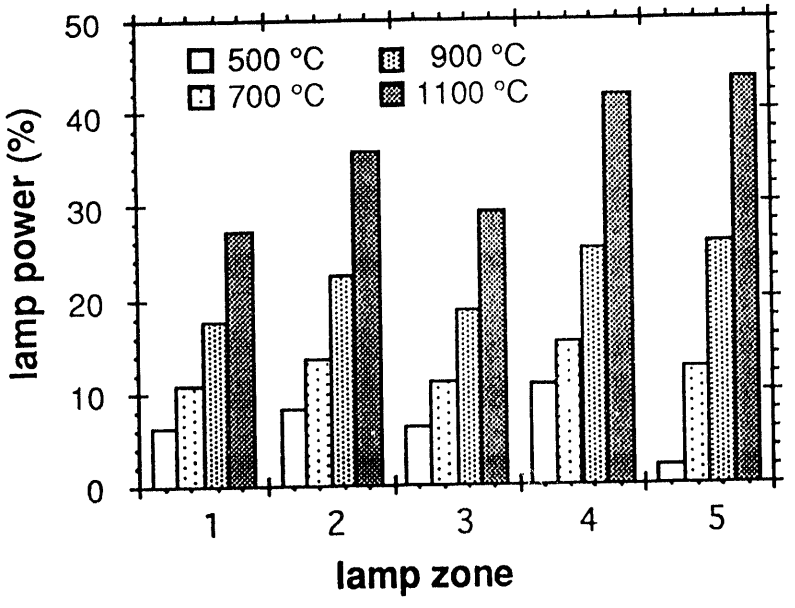

Figure 11: Optimized power levels required for optimized temperature profiles at 500, 700, 900, and 1100 °C.

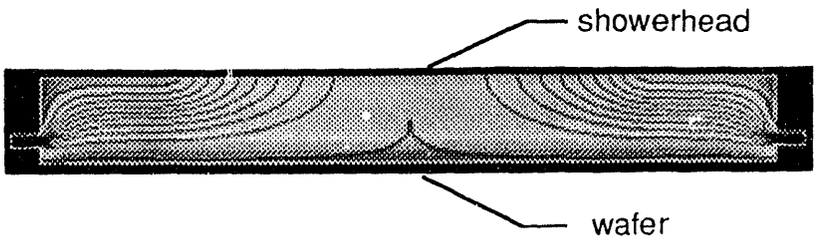

Figure 12a: Streamlines and temperature fields for reaction chamber with an inlet-to-wafer distance of 0.5 inches. Process conditions: Gas = O_2, Flow = 5 slpm, V_i = 16.1 cm/s, D_i = 8 inches, T_i = 180 °C, Pressure = 20 torr, T_{wafer} = 800 °C, Gr/Re^2 = 0.7.

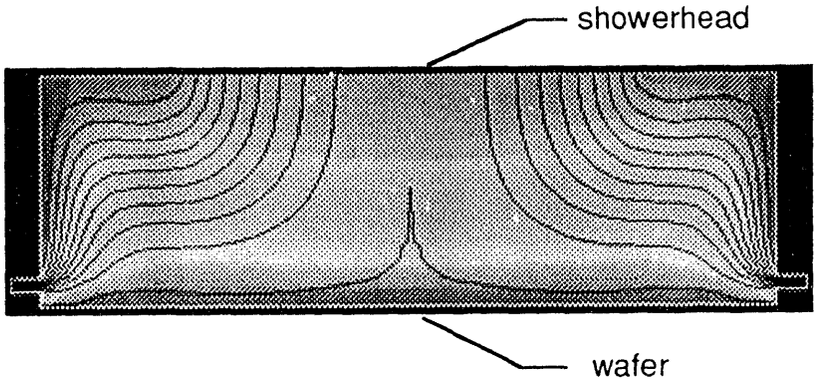

Figure 12b: Streamlines and temperature fields for reaction chamber with an inlet-to-wafer distance of 4 inches. Process conditions: Gas = O_2, Flow = 5 slpm, V_i = 16.1 cm/s, D_i = 8 inches, T_i = 180 °C, Pressure = 20 torr, T_{wafer} = 800 °C, Gr/Re^2 = 13.

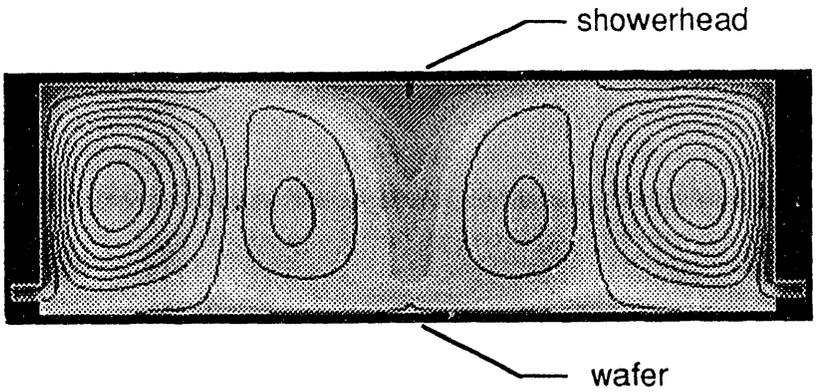

Figure 12c: Streamlines and temperature fields for reaction chamber with an inlet-to-wafer distance of 4 inches. Process conditions: Gas = O_2, Flow = 5 slpm, V_i =

3.22 cm/s, D_i = 8 inches, T_i = 180 °C, Pressure = 100 torr, T_{wafer} = 1000 °C, Gr/Re^2 = 441.

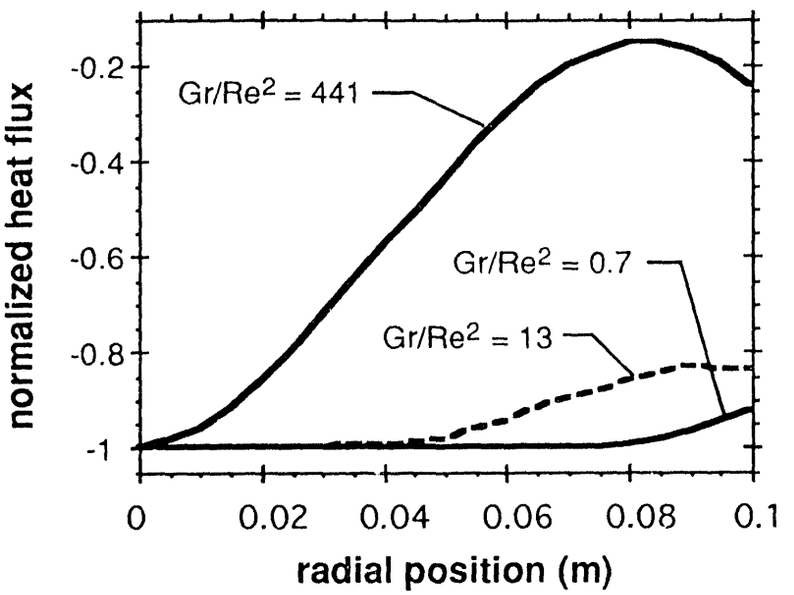

Figure 13: Predicted heat flux profiles at wafer surface for the three process conditions shown in figures 12a, 12b, and 12c.

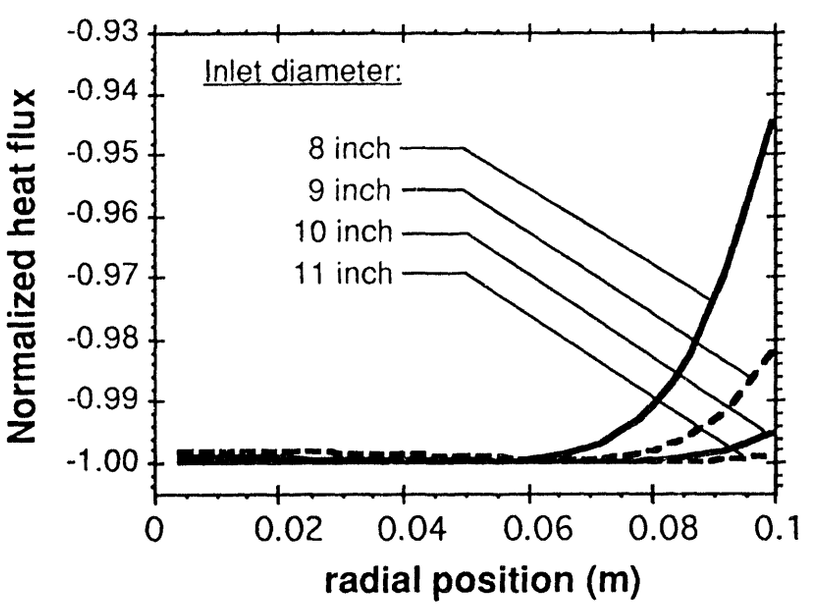

Figure 14: Normalized wafer heat flux profiles for four inlet diameters. Conditions: Gas = O_2, Flow = 5 slpm, Pressure = 20 torr, T_{wafer} = 800 °C, inlet-to-wafer distance = 1.5 inches.

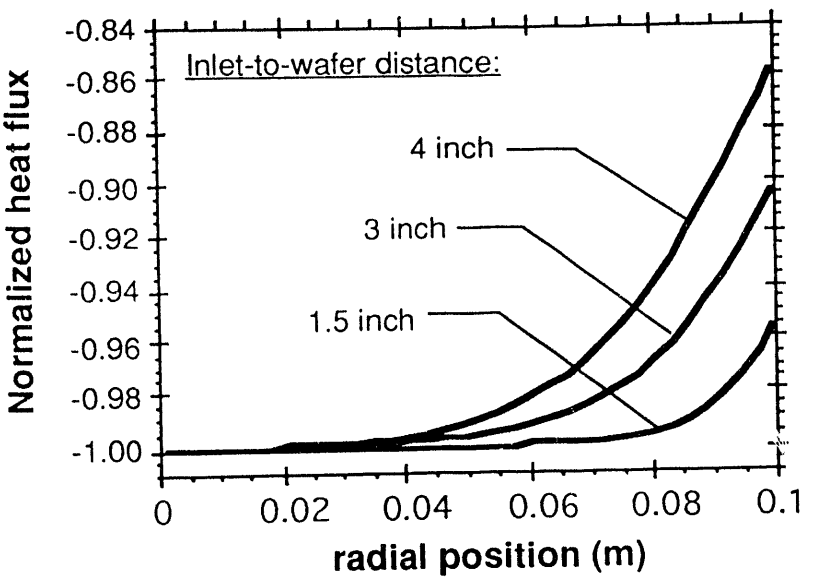

Figure 15: Normalized wafer heat flux profiles for three inlet-to-wafer distances. Conditions: Gas = O_2, Flow = 5 slpm, Pressure = 20 torr, T_{wafer} = 800 °C, inlet diameter = 8 inches.

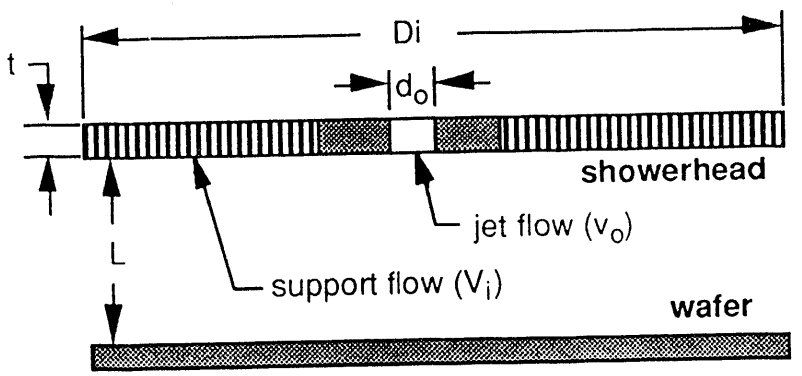

Figure 16: Parameters for showerhead hole jetting calculation.

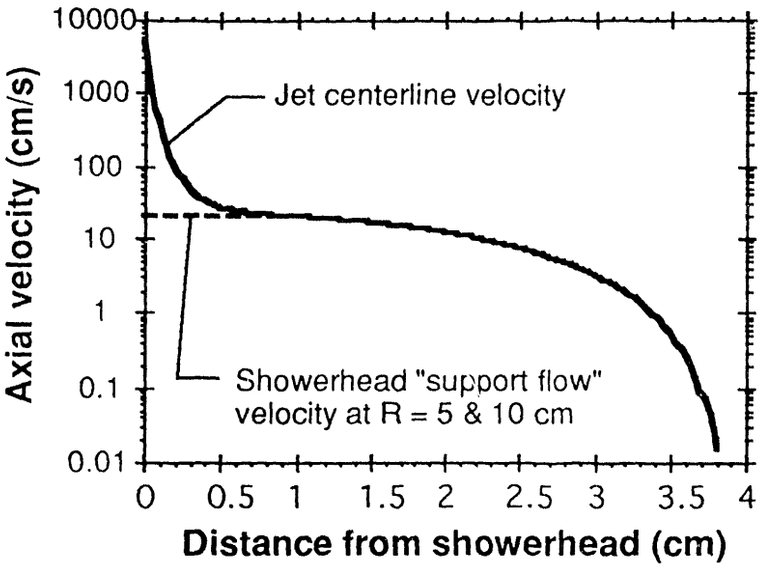

Figure 17: Comparison of jet centerline velocity and average inlet velocity as a function of distance from the showerhead surface. Conditions: Gas = O_2, Flow = 2 slpm, Pressure = 5 torr, d_o = 0.02 inches, hole spacing = 0.25 inches, inlet-to-wafer distance = 1.5 inches.

DATE
FILMED
9/26/94

END